COMBINED USE OF CONVENTIONAL GRAVITY AND SATELLITE ALTIMETRY

Paper presented at the 52 meeting of the European Association of Exploration Geophysicists, Copenhagen 28 May - 1 June 1990.

By:

C. Christian Tscherning [+], Trond Christoffersen[++] and Jon Schultzen[+++].

+ Geophysical Institute, University of Copenhagen, Haraldsgade 6, København N, Denmark.

++ AMAROK A.S., Oscars gate 46B, 0258 Oslo 2, Norway.

+++Department of Geology, University of Oslo, P.O.Box 1047 Blindern, 0316 Oslo 3, Norway.

Abstract;

The availability of a global coverage of satellite altimeter data has presented the geophysical exploration community with the possibility of obtaining satellite derived gravity data over the world oceans. This paper will look into the possibilities and limitations of using satellite altimeter measurements of the sea surface topography in combination with conventional gravity data. Both mapping and geological modelling will be considered for each data type alone and in the case of combined use.

Foundations:

The satellite altimeter records of the combined effect of geoid undulations due to gravity, sea surface topography due to oceanographic effects and various errors. From an exploration point of view the geoid is the target and the other contributions are minimized. The functional relation between geoid and gravity is briefly described, together with a description of the two selected procedures for transforming geoid data into gravity and vice versa: transformation in the space domain using least squares collocation (LSC) and transformation in the frequency domain. The advantage of the first method is it's ability to combine different types of input data in a unified modelling of the potential field. The advantage of the second method lies in the speed and efficiency offered b y the FFT, but gridded data are needed.

Mapping:

Comparisons are made of gravity maps within test areas in the Baltic Sea and off the norwegian coast. The maps types are: a) satellite altimetry transformed to gravity using LSC and b) gravity predictions based on both satellite altimetry and direct gravity measurements also using LSC. The acurracy is estimated to 3 mgal only using satellite data. The satellite data in their present state are found to be a useful supplement to detailed marine gravity, improving the mapping in areas of poor coverage, and a valuable source of regional information.

Modelling:

2-D modelling of gravity anomalies has been widely used for several decades. The analog process of 2-D modelling of geoid anomalies is described. The difference in gravity and geoid response is discussed based on computation of the model response of elementary models. The feasability of 2-D modelling of geoid anomalies versus gravity anomalies is discussed based on examples from the Norwegian Sea. The gravity and geoid response is computed for comparable 2-D geological models and plotted against the observations of conventional gravity and geoid derived from satellite altimetry.

1. Introduction

The availability of a global coverage of satellite altimeter data (GEOS-3, SEASAT, GEOSAT, and in the future ERS-1, Topex-Poseidon) has presented the exploration community with the possibility of obtaining new gravity field information over the world oceans. The altimeter data may be converted to gravity data (Rapp, 1983) or used directly in the form of geoid heights. However, in many areas at sea gravity data have already been collected, and we will here look into the possibility of combining the two types of data. In section 2 we will consider the possibilities for improving gravity field mapping and in section 3 the improvements when using the data for geological modelling.

2. Gravity Field Mapping

The satellite altimeter measures the distance from the satellite to the ocean surface. After having subtracted the height of the satellite over the ellipsoid , the observation may be written as

$$h = N + t + e \qquad (1)$$

where N is the geoid height, t the sea surface topography (tides, currents etc) and e the error, both random and due to satellite orbit errors. Using the fact that the subtracks of the orbits cross, a cross-over adjustment may be made (Rowlands, 1981, Engelis and Knudsen, 1989, Knudsen 1989) which removes (determines) t and the main part of e in eq. (1). We are then left with the geoid height.

The geoid height is related to the anomalous gravity potential, T, through Bruns equation .

$$N = T/\gamma \qquad (2)$$

where γ is the normal gravity. The free-air gravity anomaly , Δg, is also related to T in a similar simple manner,

$$\Delta g = \delta T/\delta r - 2/R\ T \qquad (3)$$

Both quantities may be expressed as a series in solid spherical harmonics, with coefficients C_{nm}, S_{nm}, see Rapp (1984). This is the equivalent of the spectrum of a Fourier series, but here on a sphere. The geoid spectrum is obtained simply by division with γ, while the gravity spectrum is obtained by multiplication with (n-1)/R, where n is the degree and R the mean earth radius. The similar relations holds if T in a local area is expanded in Fourier series using a plane approximation, see Schwarz et al. (1989).

If the Fourier spectrum of N is computed in a local area using FFT, we may then use the spectral relationship γ R/(n-1) to obtain the Fourier transformed of Δg in the same area, (Farelly and Herdlevær, 1989, Forsberg & Solheim, 1988). This naturally requires that data have been gridded in advance.

A more general method works in the space domain, similar to kriging, and is called least-squares collocation (LSC). The main difference is that the statistical properties of the signal is expressed through a covariance function, while kriging uses the variogram.

The covariance function on a sphere is expressed using a series in Legendre functions, P_n, with coefficients τ_n^2 , which corresponds to the power spectrum of a Fourier series,

$$cov_T(\psi) = \sum_{n=2}^{\infty} \tau_n^2\ P_n\ (\cos\psi) \qquad (4)$$

where ψ is the spherical distance between two observation points of T, and

$$\tau_n^2 = \sum_{m=0}^{n} (C_{nm}^2 + S_{nm}^2)\ (R\gamma)^2 \qquad (5)$$

The auto - and cross - covariance function are obtained using the spectral

relationship, or by applying eq. (2), (3), respectively on eq. (4). (We have left out a height dependent term in eq. (4) because we here only discuss quantities at sea level).

The infinitely many values of τ_n^2 are naturally not available, but are modelled using simple power functions of n, see Tscherning and Rapp (1974). The advantage of this is that the covariance function may be expressed by a closed formula.

A quantity, y, (N or Δg) may then be obtained from observations x_i , i = 1,...,n (again N and/or Δg) using

$$\tilde{y} = C_y^T \tilde{C}^{-1} x \qquad (6)$$

where C_y is the cross-covariance vector between y and the observations, $\tilde{C}$= C+D, where C is the auto-covariance of the observations and D the covariance- matrix of the noise, and x the observation vector. This is the method of least-squares collocation (Moritz, 1980), which (like Kriging) has the property that noise-free data are reproduced exactly. The method may also be used to estimate parameters like orbit biases and tilts.

As may be seen from eq. (6), a solution of a system of equations is necessary. This makes the method much slower to use than the FFT-based method. However, we may directly combine data of different kinds, and also compute error estimates,

$$\sigma_n^2 (y - \tilde{y}) = C_0 - C_y^T \tilde{C}^{-1} C_y \qquad (7)$$

where C_0 is the variance of y.

The method has been used with SEASAT data in two areas in the Baltic Sea and one in the Norwegian Sea, where we computed the geoid and the free-air gravity anomalies using only satellite altimetry and by a combination with gravity observations, see Fig. 1-3, 6-8, 11-13. Also the error estimates were calculated using eq. (7). Using only altimeter data, the best results are found (as should be

expected) in areas with much observations, see Fig. 4,9,14. A direct comparison with observed sea-gravity of high quality was only possible in the Norwegian Sea, (Fig. 16), where we could verify the small error of only 2 - 3 mgal.

A combination with observed gravity anomalies naturally made the error decrease to the noise level of the observations (0.5 - 1 mgal when best), but also the error in areas with no gravity data decreased slightly. Note, that the total gravity variation in the area was only +/- 7.6 mgal, so the maximal error will have this magnitude. This small range of values was obtained by subtracting in advance the contribution from a spherical harmonic expansion complete to degree 360, and subsequently adding the effect to the result.

The difference between satellite and marine gravity will to some extent depend on the frequency and amplitude of the anomalies, where the resolution of more high frequent anomalies is inferior in the satellite data. It has been estimated that the highest freqency fully represented in the satellite altimetry is 3 cycles/degree or approximately 37 km (Knudsen, 1989). The reason for this is mainly the spacing between the satellite tracks, but also the 7 km foot print (1 sec sample rate) for most satellite data. Possible improvements may be obtained by utilizing the 0.1 sec sample rate now available from GEOSAT and from the launching of new sattelites that will improve the spatial coverage .

3. Combined gravity and geoid modelling.

The contribution to the geoid from a single body of constant density is

$$N = -G\rho/\gamma \int_V 1/r \; dV \qquad (8)$$

where G is the newtonian constant of gravitation, ρ the density of the body, γ the normal gravity, V the volume of the body and r the distance from the observaition point to the volume element dV. The contribution of the same body to the gravity anomaly (measured in the vertical direction) is

$$\Delta g = -G\rho \int_V \cos\phi/r^2 \; dV \qquad (9)$$

where ϕ is the angle between the vertical and the vector from the observation to the volume element.

The solution of eq.(9) by line integral methods for 2-D bodies (Talwani and Ewing, 1960) provided the basis for the most frequently used method in gravity interpretation: forward 2-D computer modelling, later accompanied by its 3-D and 2.5-D equivalents. With the availability of global coverage of high quality geoid height measurements, it seems worth while to produce similar modelling tools for this quantity. It can be shown that the geoid anomaly produced by a 2-D body of constant density is (Schultzen, in prep.):

$$N = - G\rho / \gamma \int r^2 (\ln r - 0.5)\, d\theta \qquad (10)$$

in polar coordinates where r is the distance from the observation point to the line element and θ the angle. Eq (10) has been implemented on a computer to allow simultaneous modelling of the gravity and geoid response of a model. The following examples have been made using this software.

Both Δg and N depends only on the density (ρ) and the model geometry. This means that in many cases two independent sets of observations are available which both are a function of the same geological model parameters. As Δg is proportional to $1/r^2$ (eq.(9)) and N is proportional to 1/r (eq.(8)) when r is the distance to the disturbing mass, gravity is more sensitive to shallow contrasts and the geoid is more sensitive to deeper contrasts. This may be of benefit to the final model.

It is important to bear in mind that the functional relation between Δg and N means that simultaneous gravity and geoid modelling does not resolve the ambiguity of gravity modelling. Two different bodies producing the same gravity anomaly will also produce the same geoid anomaly (Fig 17). The possible practical benefit from this approach will be a result of the different frequency content in the two sets of measurements. Especially the attention to the geoid may contribute to improved control with the regional effects thereby limiting the available possibilities in the traditional modelling of the residual field.

As a test area for the geological modelling we wanted to select an area with large scale tectonic features, but also well enough explored to provide some structural control for the modelling. The profile selected is C-165, a 700 km long transect crossing the norwegian Vøring margin. The location is shown superimposed on the Seasat geoid anomalies in the area (Fig.18). The main trend in the geoid data is SW-NE sufficiently perpendicular to C-165 to make 2-D modelling reasonable.

An interpreted cross-section of C-165 (Skogseid and Eldholm, 1989) shows the main structural elements of the Nordland continental shelf and the Vøring Plateau (Fig. 19). The cross section combines the shallow crustal structure from the seismic line, the deep crustal velocity structure from refraction work by ESP (Expanding Spread Profiles) and sonobouys, and gravity information (Planke et al., in press).

A gravity model was constructed for this line (Fig. 20). We first chose to infer the deep part of this model from the iso-velocity horizons of Fig 19. We tentatively associated the 8.1 km/s horizon with a crust/mantle density contrast, and adjusted the geological model to produce a fit between observed and calculated gravity. A test of the geoid response of this model revealed fundamental mismatch with the observations. The moho undulations at 100 km (along the profile) produce a negative geoid anomaly where a positive anomaly is observed. East of 300 km the geoid response of the model drops more than 15 meters while the observations decrease less than 4 meters.

If we assume no density contrast at all across the 8.1 km/s horizon, the geoid response becomes of the same order of magnitude as the observations, but the gravity response is no longer correct (Fig. 21). The source of the erroneous geoid response is clearly shown when we compute separately the effect of the tentative moho in the original model (Fig 22).

Isostasy obviously is a keyword when geoid anomalies are to be modelled. An uncompensated 15 km change in moho depth over a 600 km distance produces a geoid anomaly of more than 25 meters (Fig 23). This figure also shows that geoid models are very sensitive to edge effects and that care should be taken as far as 100 km from the edge of the model, depending on the contrasts involved and the depth of the structure.

Based on the geometry of the initial model, a crust/mantle interface was computed assuming Airy-type isostatic equilibrium (Fig. 24). The correlation between this surface and the moho tentatively inferred from the 8.1 iso-velocity horizon is very poor. The next modelling steps will aim at producing a reasonable isostatic model that also is in agreement with observed gravity and geoid anomalies. The gradient of the geoid anomaly invited to make modifications in the crustal model east of 300 km where the heavy deep rocks modelled at 2.9 g/cm^3 were assumed to rise gradually shallower when approaching land. This is compatible with the outcropping gneisses and amphibolites onshore. A new airy-type moho was computed based on this revised crustal model and an assumed average crustal thickness under the continental shelf of 27 km (Fig 25). These assumptions lead to an increase of crustal thickness to more than 35 km onshore and a significant thinning west of the transition to assumed normal oceanic crust at 100 km. A root compensation under the Bodø High at 300 km is obviously exaggerated due to the zero flexural rigidity in the Airy computations, and our first selection of a new moho allows three basic levels corresponding to oceanic crust, the continental shelf and onshore Norway.

The introduction of the above modifications into the model improves the model-response significantly and the errors are now less than an order of magnitude. This improvement is achieved even though the gravity response is wrong, the geoid response is wrong and the rules of isostasy are not strictly obeyed, (Fig 26). We see that both the gravity and the geoid response is too small over the Bodø High at 300 km due to the rejection of a "mantle-intrusion", and also that there is not enough negative mass in the Helgeland Basin at 450 km.

To improve the model, the deep parts of the Bodø High basement high was broadened to allow heavy basement rocks to make up for the rejected "mantle-intrusion". Also a "mini-root" was introduced to take up part of the Bodø High load, the basement high itself was made broader and an increasing sediment thickness was introduced in the Helgeland Basin. This results in large improvements in the fit between model response and observations (Fig 27).

A final iteration is made to improve the fit and take better care of the correspondence between this model and mapped geology in the upper 5 km (Fig

28). The fact that the geoid modelling has been performed in 2-D means that the model response becomes an over-estimate compared to a 2 1/2-D or 3-D geoid model. This is especially true in the upper crust where very few structures preserves a stable geometry for e.g. 50 km. Given these limitations the results of this regional modelling may be of some interest to the regional understanding of the area. It may itself be revised, refined or serve as a regional background for more detailed local modelling.

Conclusions:

We see that:

(1) The satellite altimetry gives high quality gravity information. In the test area with best coverage of marine gravity data (SW Barents Sea) the difference between satellite derived and conventional gravity is 2-3 mGal.

(2) The ability of the method of least squares collocation to combine altimetry and conventional gravity is attractive in areas where good conventional gravity coverage is only partly available.

(3) Spatial resolution which is currently the weak point of satellite altimetry is expected to improve with the improvement in spatial coverage from new satellites like the ERS-1.

(4) When both gravity and geoid anomalies are avaliable simultaneous modelling can improve the control of regional effects.

(5) Modelling of shallower structures can also benefit from the increased control in simultaneous modelling.

Acknowledgements:

The authors wish to thank J. Skogseid, O. Eldholm and S. Planke for the permission to use their interpretation of the regional transect C-165, and to thank Statoil for its positive attitude towards using experience gained in previuous modelling work. The first author thanks Norsk Hydro Udforskning (DK) for support in this field.

References:

Engelis, T. and P. Knudsen: Orbit improvement and determination of the Ocean Geoid and Topography from 17 days of Sesat Data. Manuscripta Geodaetica. Vol. 14 no 3, pp. 193-201, 1989.

Farelly, B and A Herdlevær: Comparison of FFT and Other Methods for Treatment of Satellite Altimeter Data. Report BAF891024, Norsk Hydro A/S, Bergen, E&P Research Centre, 1989.

Forsberg, R. and D. Solheim: Performance of FFT methods in local gravity field modelling. Proceedings Chapman Conference on Progress in the Determination of the Earths Gravity Field, Ft. Lauderdale, Sept. 13-16, 1988, pp. 100-103, American Geophysical Union, 1988.

Knudsen, P.: Simultaneous estimation of the gravity field and sea surface topography from satellite altimeter data by least squares collocation. Submitted Geophys. J. Int., 1989.

Moritz, H.: Advanced Physical Geodesy. H. Wichmann Verlag, Karlsruhe, 1980.

Planke, S., J. Skogseid, and O. Eldholm: Crustal structure off Norway, 62 deg. - 70 deg. N. Techtonophysics, in press.

Rapp, R.H.: The Determination of Geoid Undulations and Gravity anomalies from SEASAT Altimeter Data. J. Geophys. Res., Vol. 88, No. C3, pp. 1552-1562, 1983.

Rapp, R.H.: The Determination of high degree potential coefficient expansions from the combination of satellite and terrestrial gravity information. Reports of the Dep. of Geodetic Science and Surveying, No. 361, The Ohio State University, Columbus, 1984.

Rowlands, D.: The Adjustment of SEASAT Altimeter Data on a Global Basis for Geoid and Sea Surface Height Determinations. Reports of the Department of

Geodetic Science and Surveying, no. 325. The Ohio State University, Columbus, 1981.

Schultzen, J: Cand Scient thesis, Dept. of Geology, University of Oslo, in prep.

Schwarz, K.P., M.G. Sideris and R. Forsberg: The use of FFT techniques in physical geodesy. Submitted for publication, 1989.

Skogseid, J. and O. Eldholm: Vøring Continental Margin: seismic interpretation, stratigraphy and vertical movements. In Eldholm, O., J. Thiede, E. Taylor, et al., Proc. ODP, Sci. Result, 104: Collece Station, Texas, (Ocean Drilling Program), 993-1030, 1989.

Talwani, M. and M. Ewing: Rapid gravity computations for two dimensional bodies with application to the Mendocino submarine fracture zone. J.Geophys.Res.,Vol 64, pp 49-59, 1960.

Tscherning, C.C. and R.H. Rapp: Closed Covariance Expressions for Gravity Anamalies, Geoid Undulations, and Deflections of the Vertical Implied by Anamaly Degree-Variance Models. Reports of the Department of Geodetic Science No. 208, The Ohio State University, Columbus, Ohio, 1974.

AREA:
BALTIC SEA 1

FIG 1

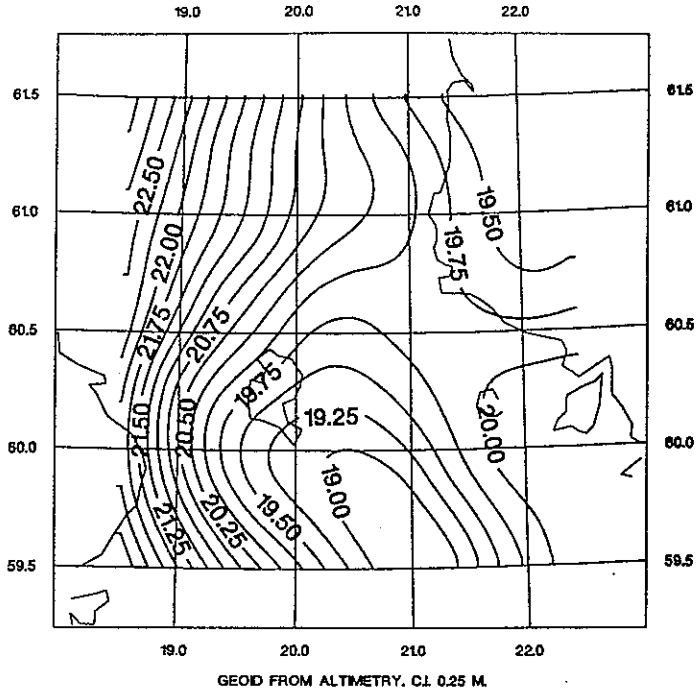

GEOID FROM ALTIMETRY. C.I. 0.25 M.

FIG 2

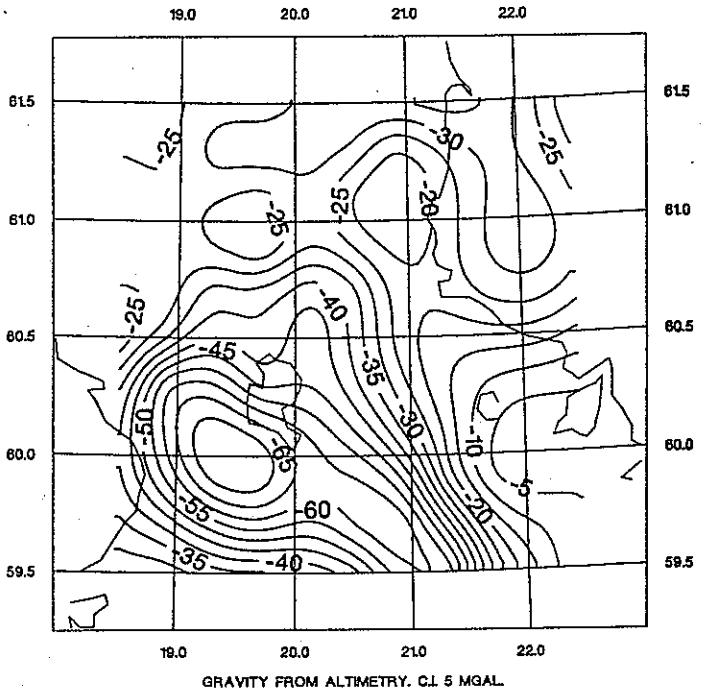

GRAVITY FROM ALTIMETRY. C.I. 5 MGAL.

FIG 3

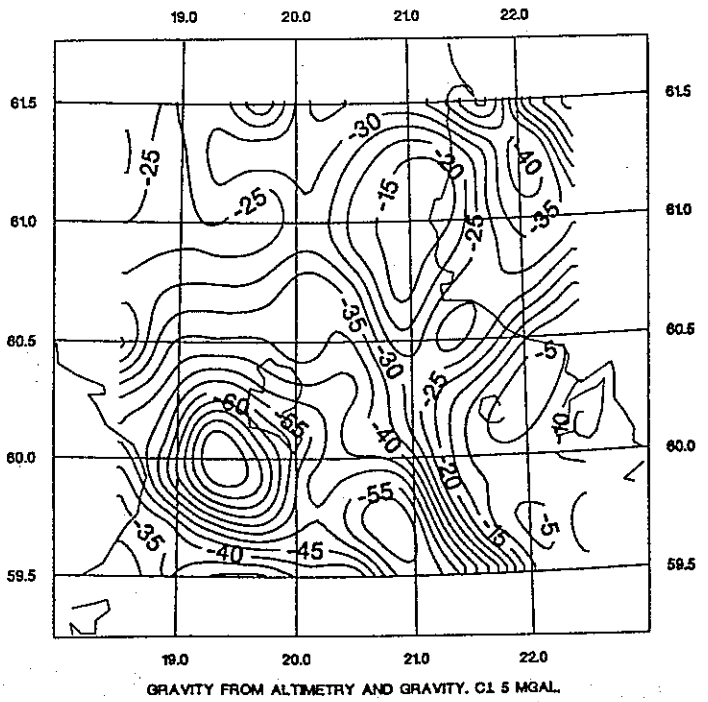

GRAVITY FROM ALTIMETRY AND GRAVITY. C.I. 5 MGAL.

AREA:
BALTIC SEA 1

FIG 4

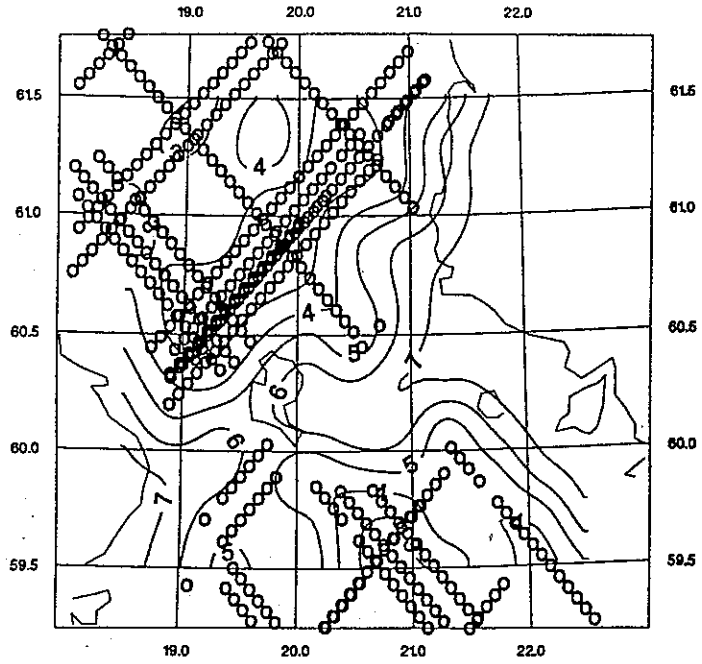

ERROR OF GRAVITY FROM ALTIMETRY, C.I. 1 MGAL, AND ALTIMETRY.

FIG 5

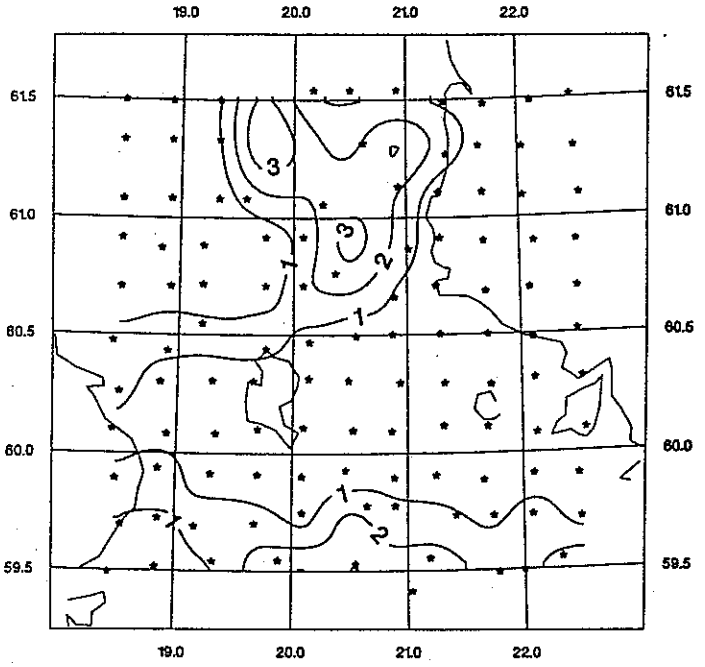

ERROR OF GRAVITY FROM ALTIMETRY AND GRAVITY, C.I. 1 MGAL, AND GRAVITY.

AREA:
BALTIC SEA 2

FIG 6

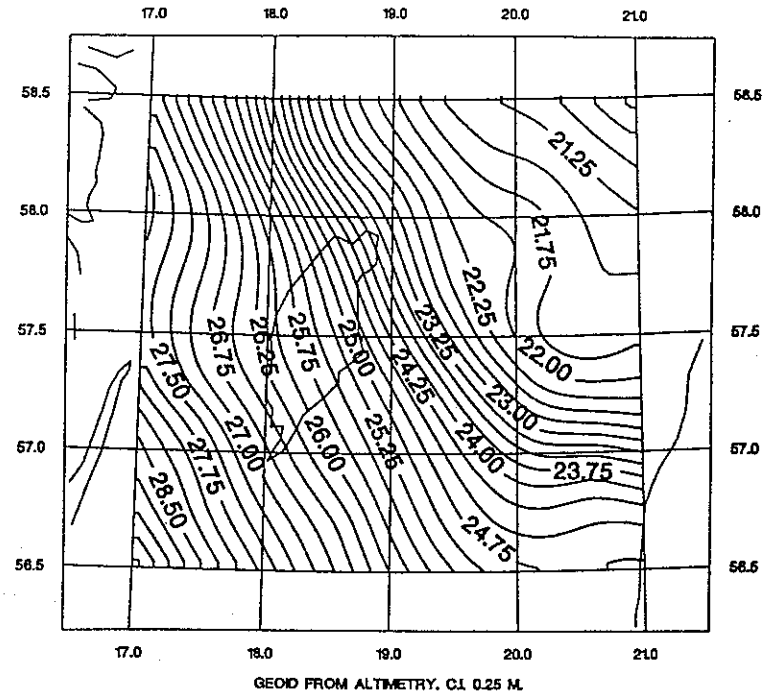

GEOID FROM ALTIMETRY. C.I. 0.25 M.

FIG 7

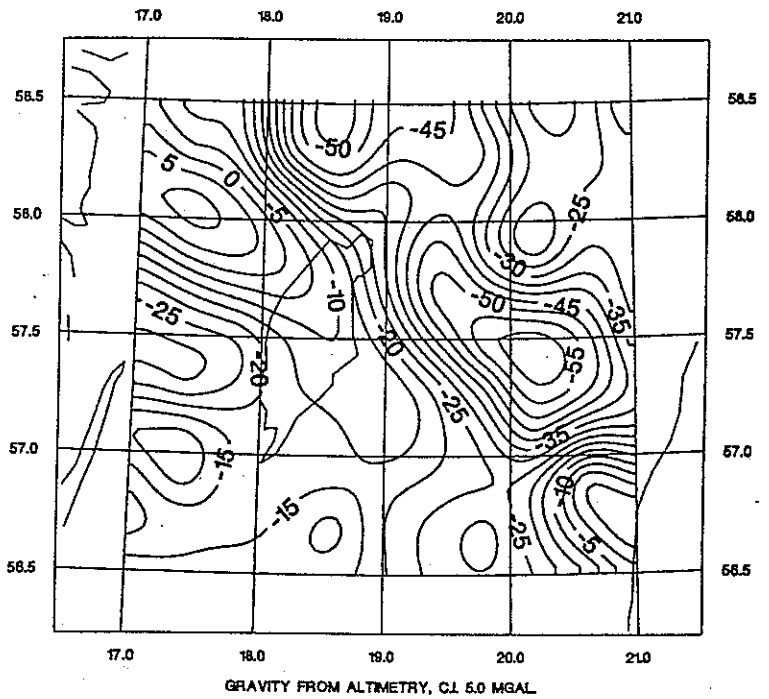

GRAVITY FROM ALTIMETRY, C.I. 5.0 MGAL.

FIG 8

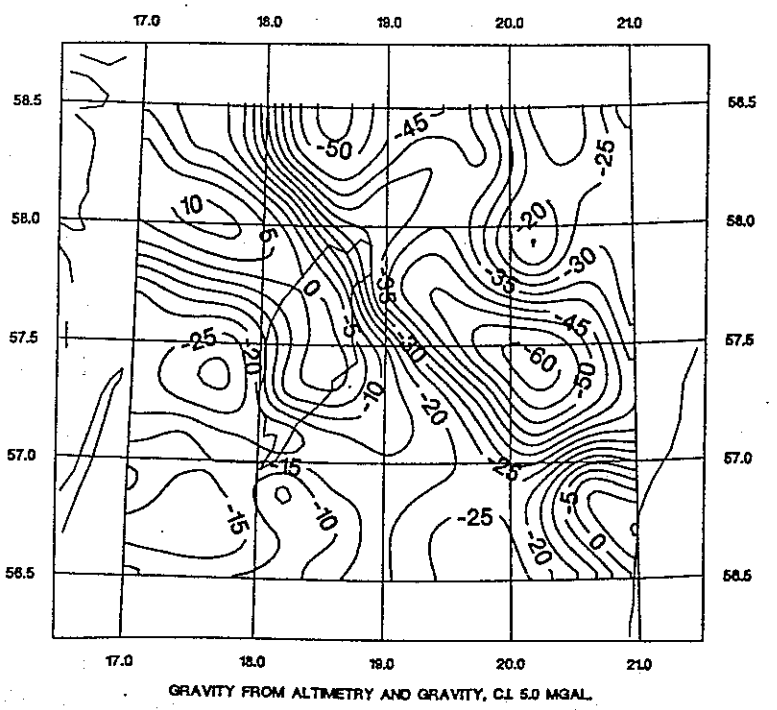

GRAVITY FROM ALTIMETRY AND GRAVITY, C.I. 5.0 MGAL.

AREA:
BALTIC SEA 2

FIG 9

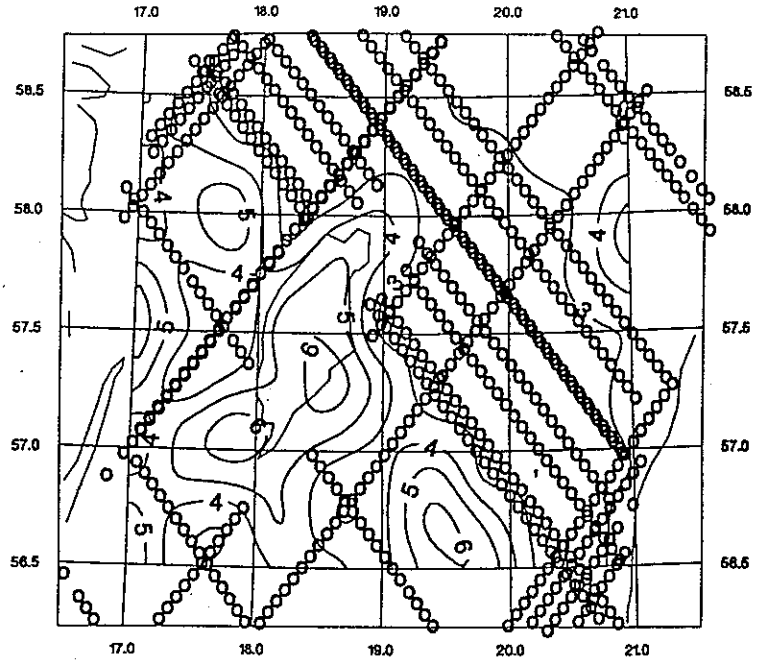

ERROR OF GRAVITY FROM ALTIMETRY, C.I. 1.0 MGAL.

FIG 10

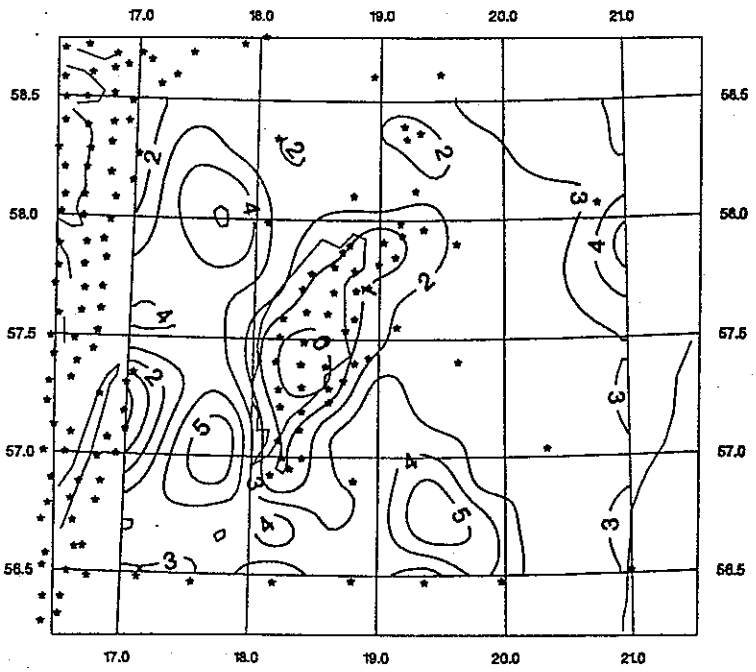

ERROR OF GRAVITY FROM ALTIMETRY AND GRAVITY, C.I. 1.0 MGAL, AND GRAVITY.

AREA:
BARENTS SEA

FIG 11

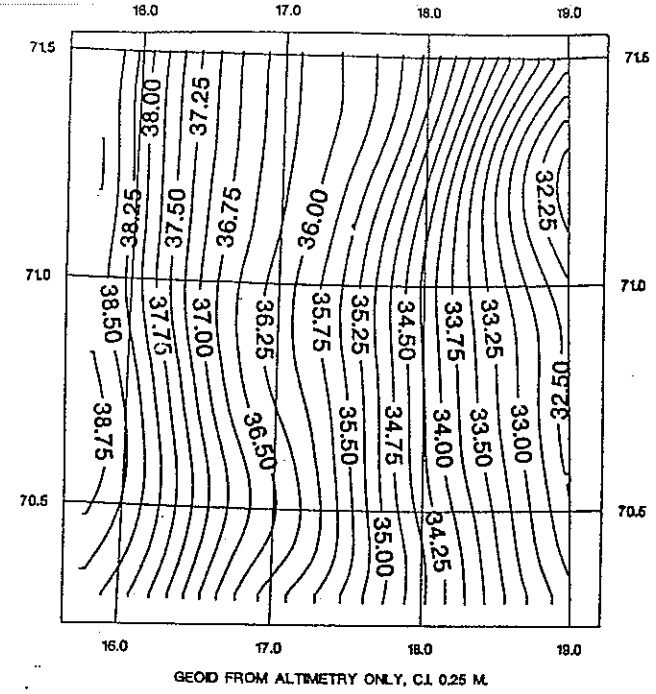

GEOID FROM ALTIMETRY ONLY, C.I. 0.25 M.

FIG 12

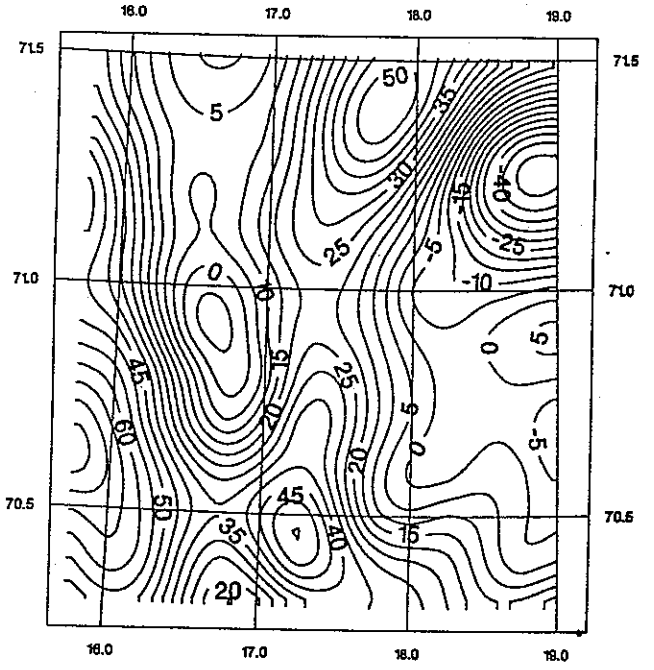

GRAVITY FROM ALTIMETRY ONLY, C.I. 5 MGAL.

FIG 13

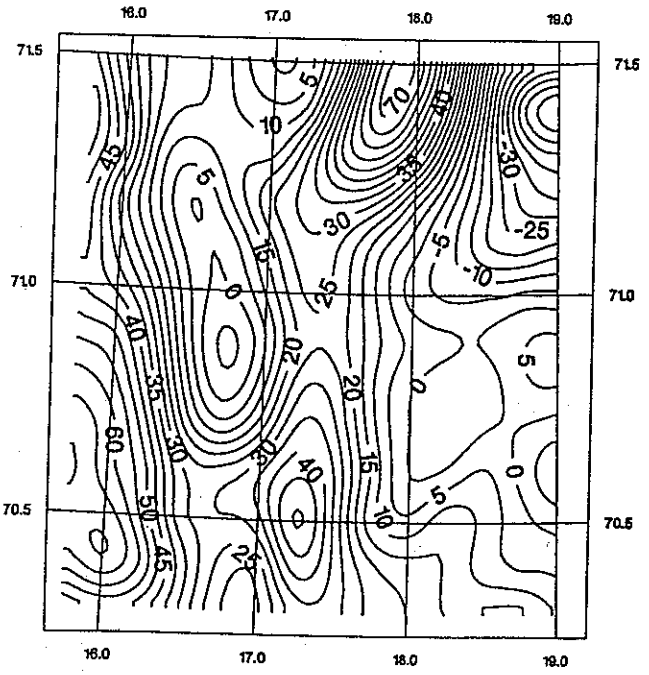

GRAVITY FROM ALTIMETRY AND GRAVITY, C.I. 5 MGAL.

AREA:
BARENTS SEA

FIG 14

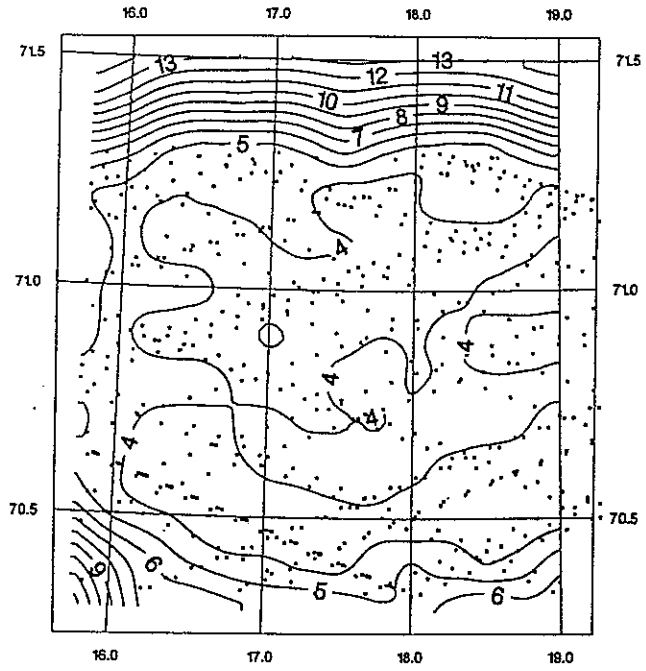

ERROR OF GRAVITY FROM ALTIMETRY ONLY, C.I. 1 MGAL, AND ALTIMETRY.

FIG 15

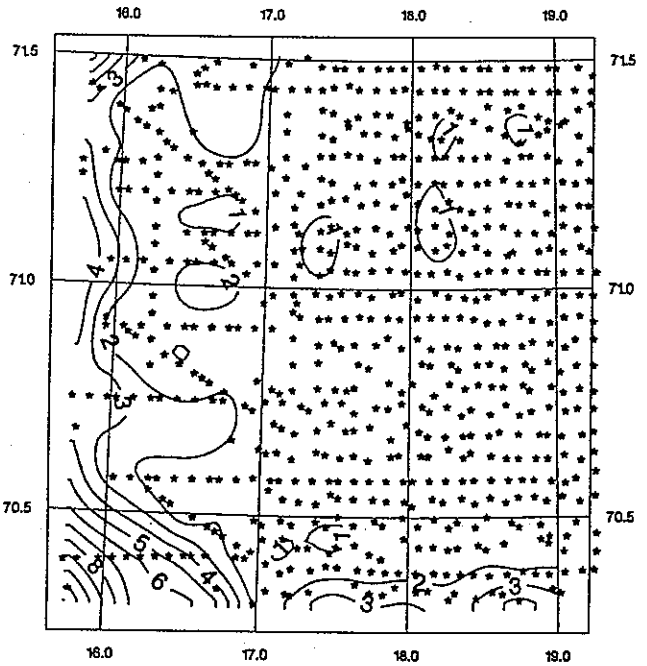

ERROR OF GRAVITY FROM ALTIMETRY AND GRAVITY, C.I. 1 MGAL, AND GRAVITY.

FIG 16

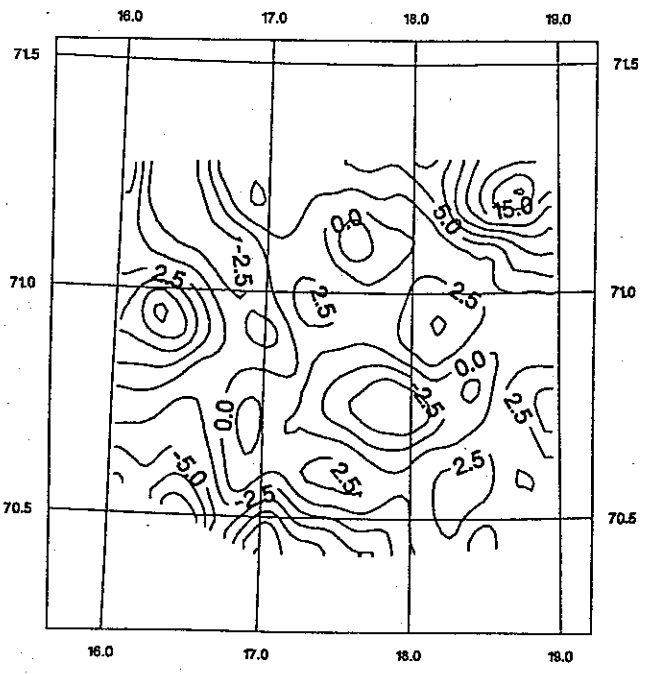

DIFFERENCE (NEW) OBSERVED - COMPUTED GRAVITY FROM ALT., C.I. 2.5 MGAL.

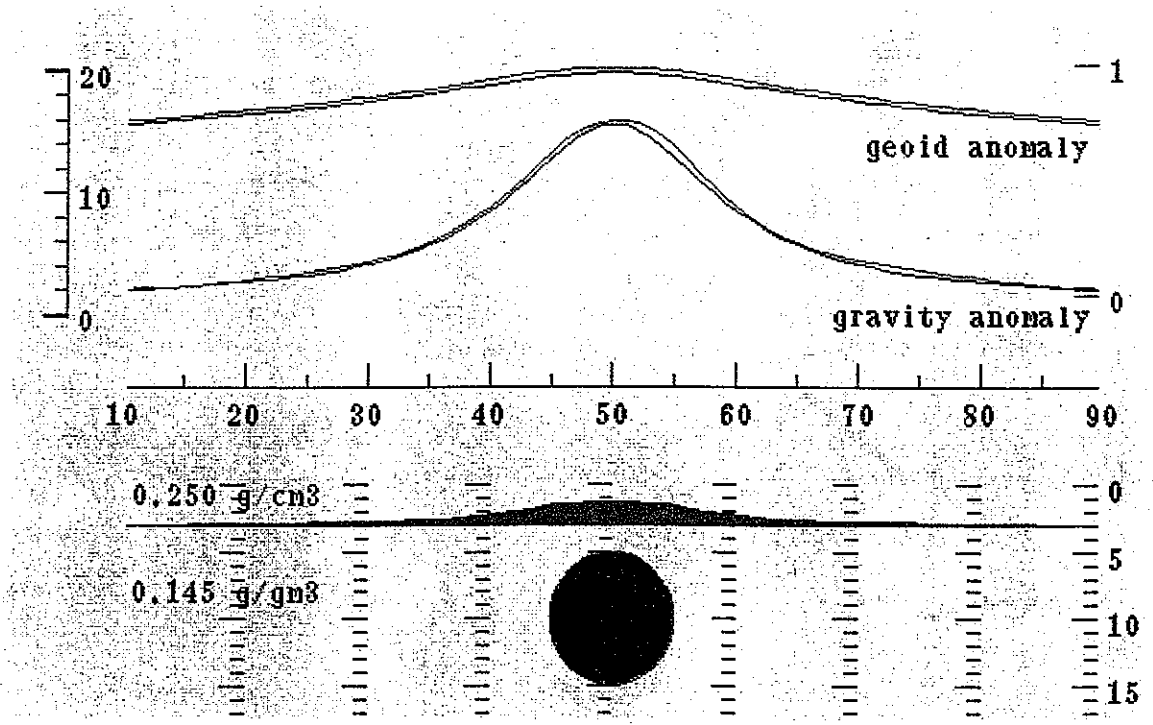
20
10
0
1
geoid anomaly
gravity anomaly
0
10
20
30
40
50
60
70
80
90
0.250 g/cm3
0.145 g/gm3
0
5
10
15

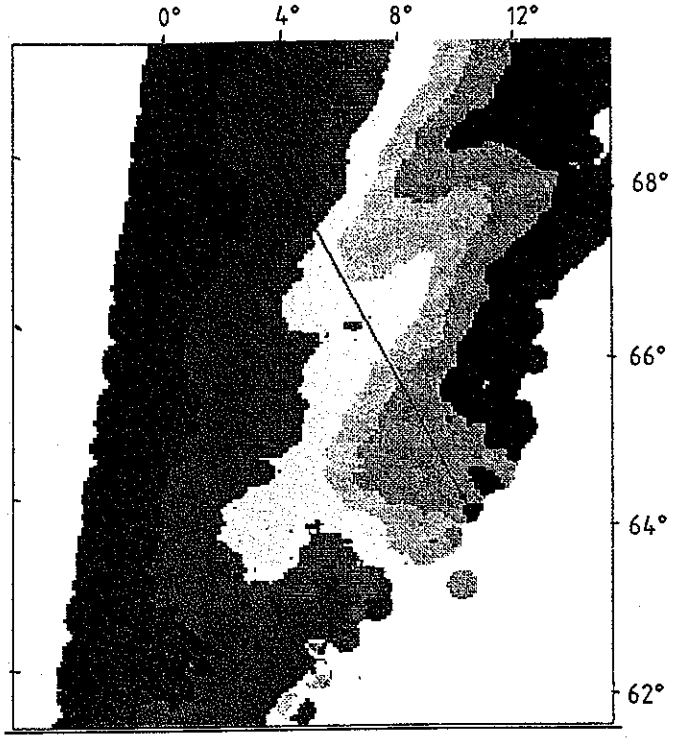

FIG 18

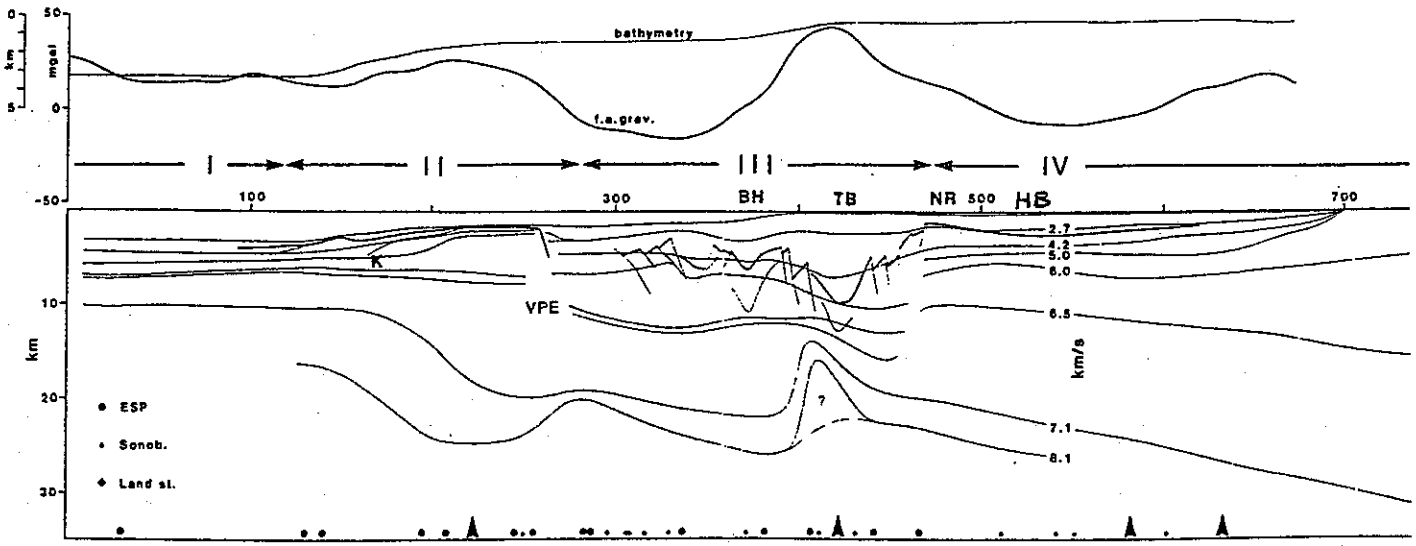

FIG 19. line C-165. VPE =Vøring Plateau ESC, BH = Bodø High, TB = Træna Basin, NR = Nordland Ridge, HB = Helgeland Basin

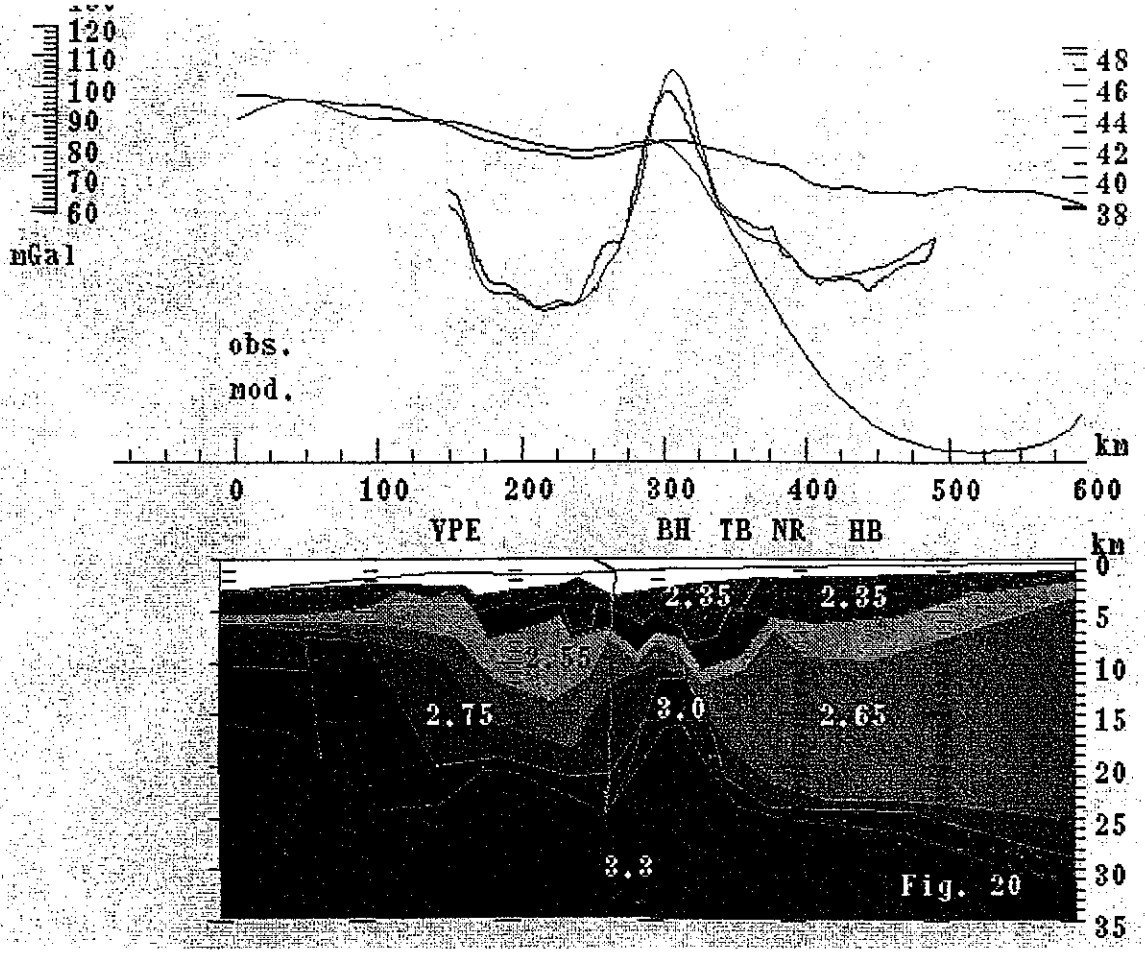
120
110
100
90
80
70
60
mGal
48
46
44
42
40
38
obs.
mod.
km
0
100
200
300
400
500
600
VPE
BH TB NR HB
km
0
5
10
15
20
25
30
35
2.35
2.35
2.55
2.75
3.0
2.65
3.3

Fig. 20

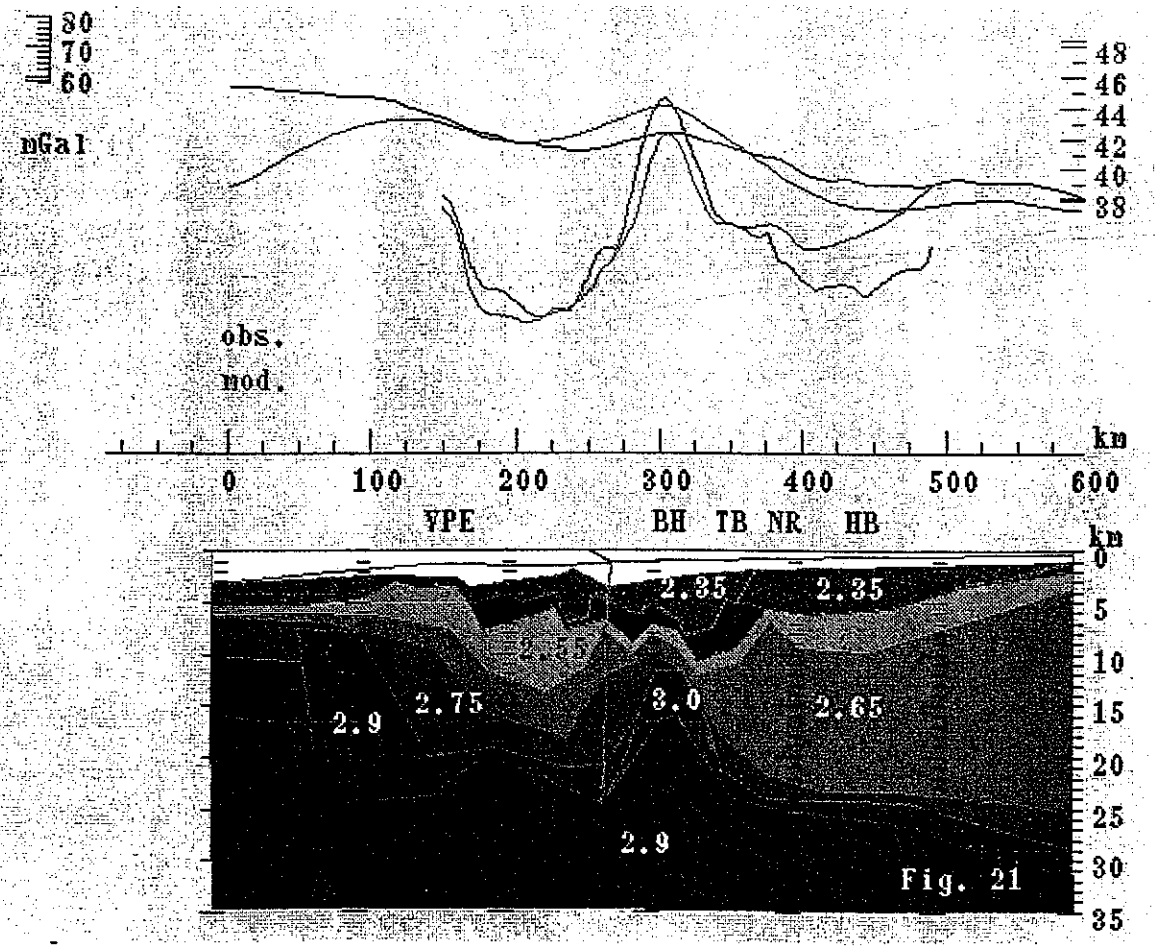
80
70
60
mGal
48
46
44
42
40
38
obs.
mod.
km
0
100
200
300
400
500
600
VPE
BH TB NR HB
km
0
5
10
15
20
25
30
35
2.35
2.35
2.55
2.9
2.75
3.0
2.65
2.9

Fig. 21

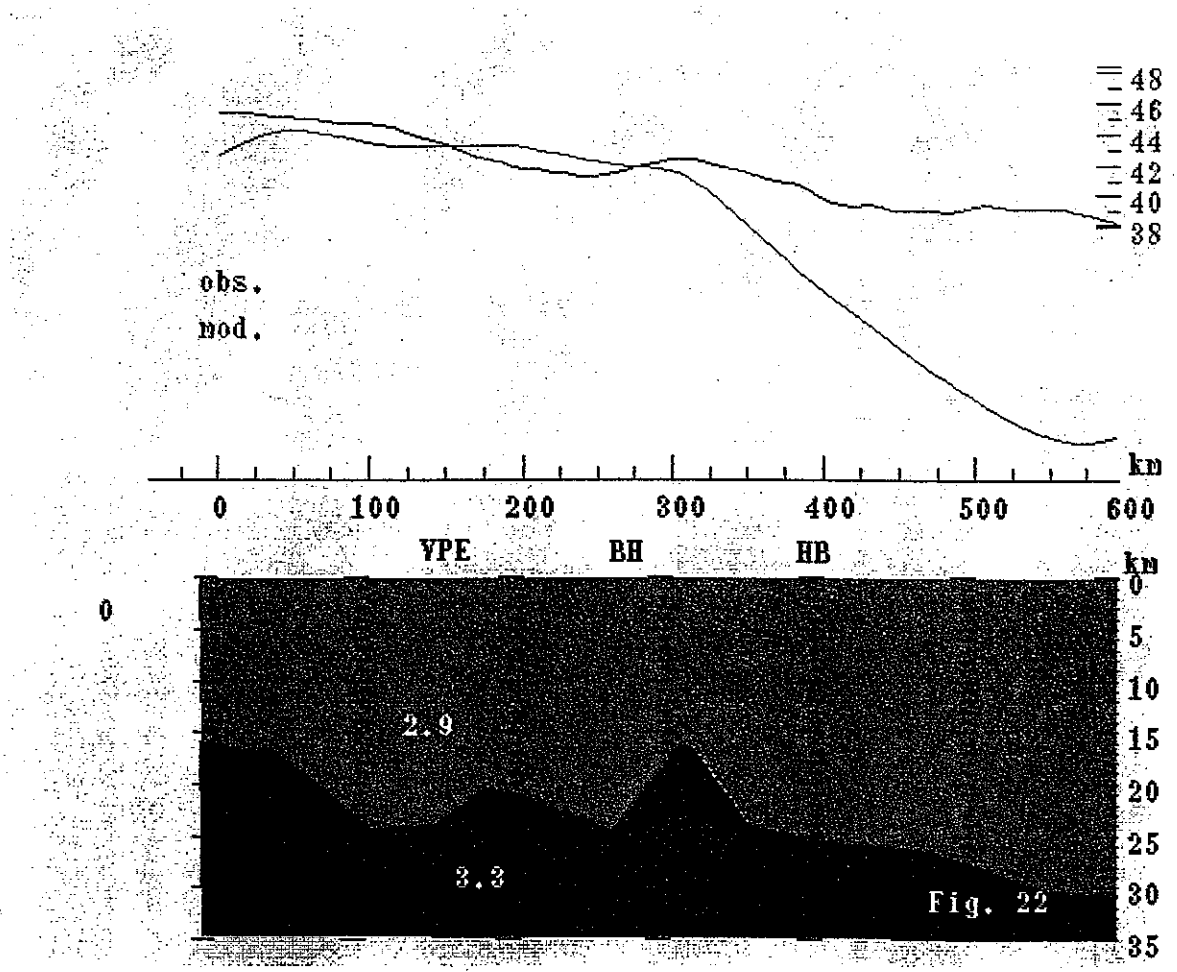
48
46
44
42
40
38
obs.
mod.
km
0
100
200
300
400
500
600
VPE
BH
HB
km
0
0
5
10
15
20
25
30
35
2.9
3.3

Fig. 22

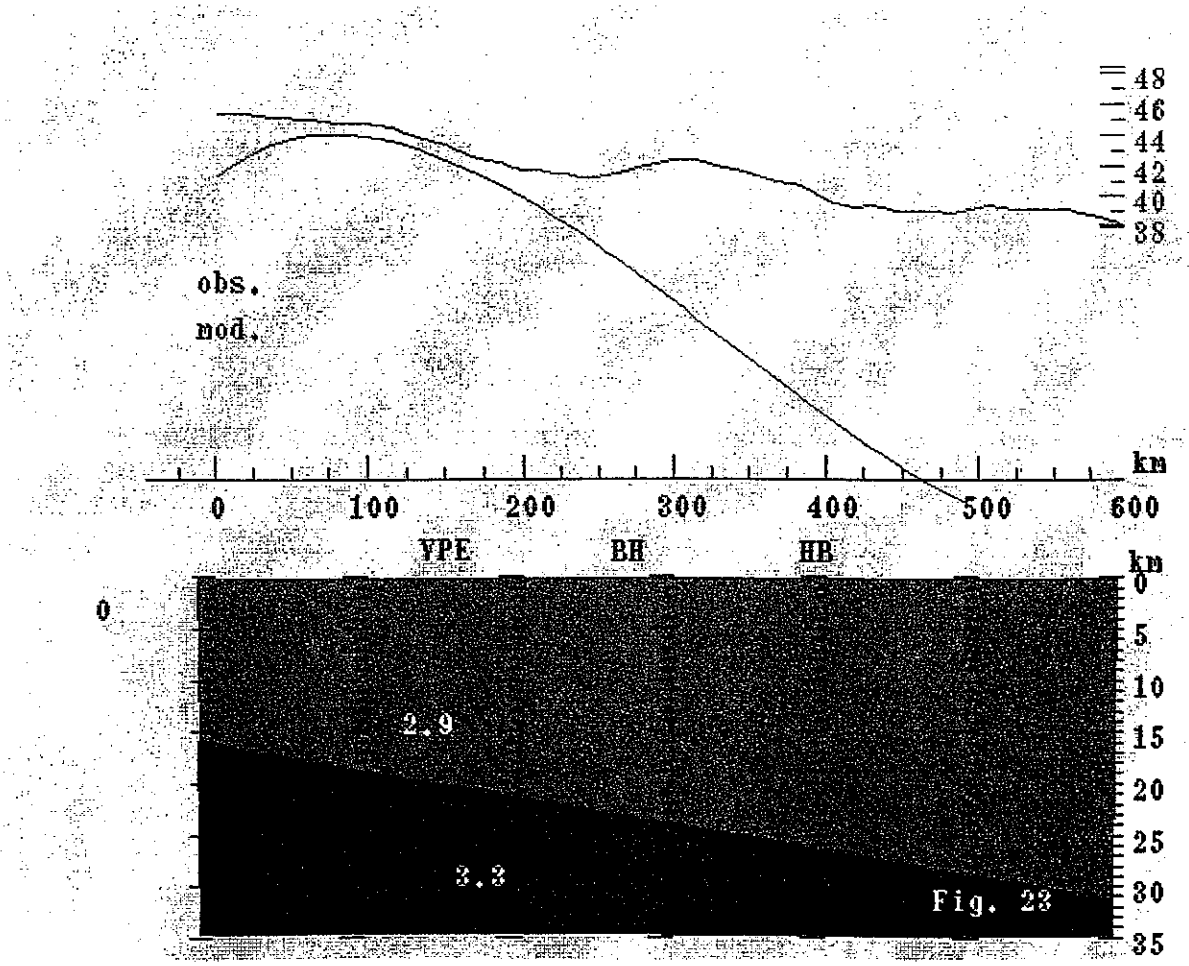
48
46
44
42
40
38
obs.
mod.
km
0
100
200
300
400
500
600
VPE
BH
HB
km
0
0
5
10
15
20
25
30
35
2.9
3.3

Fig. 23

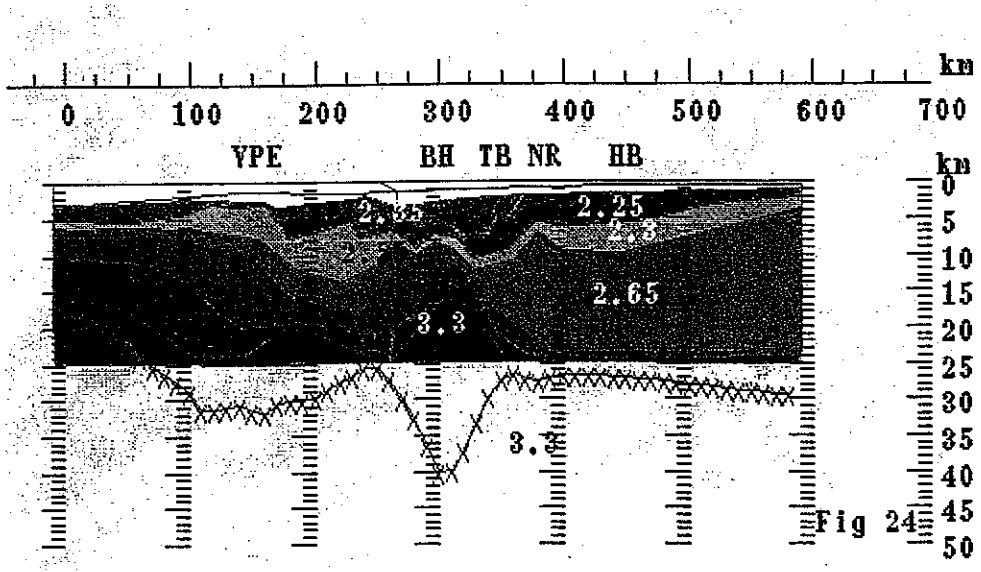
km
0
100
200
300
400
500
600
700
VPE
BH TB NR HB
km
0
5
10
15
20
25
30
35
40
45
50
2.25
2.3
2.65
3.3

Fig 24

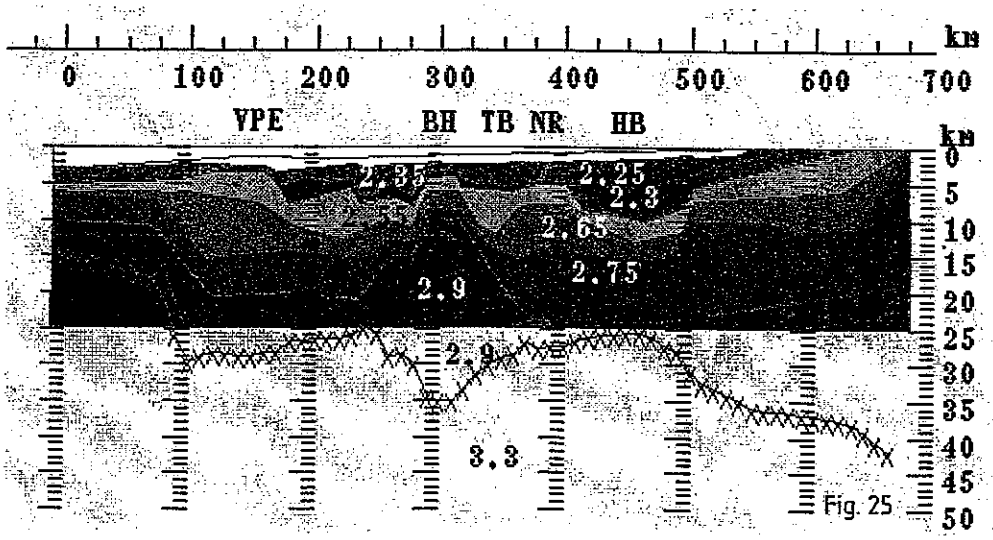
km
0
100
200
300
400
500
600
700
VPE
BH TB NR HB
km
0
5
10
15
20
25
30
35
40
45
50
2.25
2.3
2.65
2.75
2.9
3.3

Fig. 25

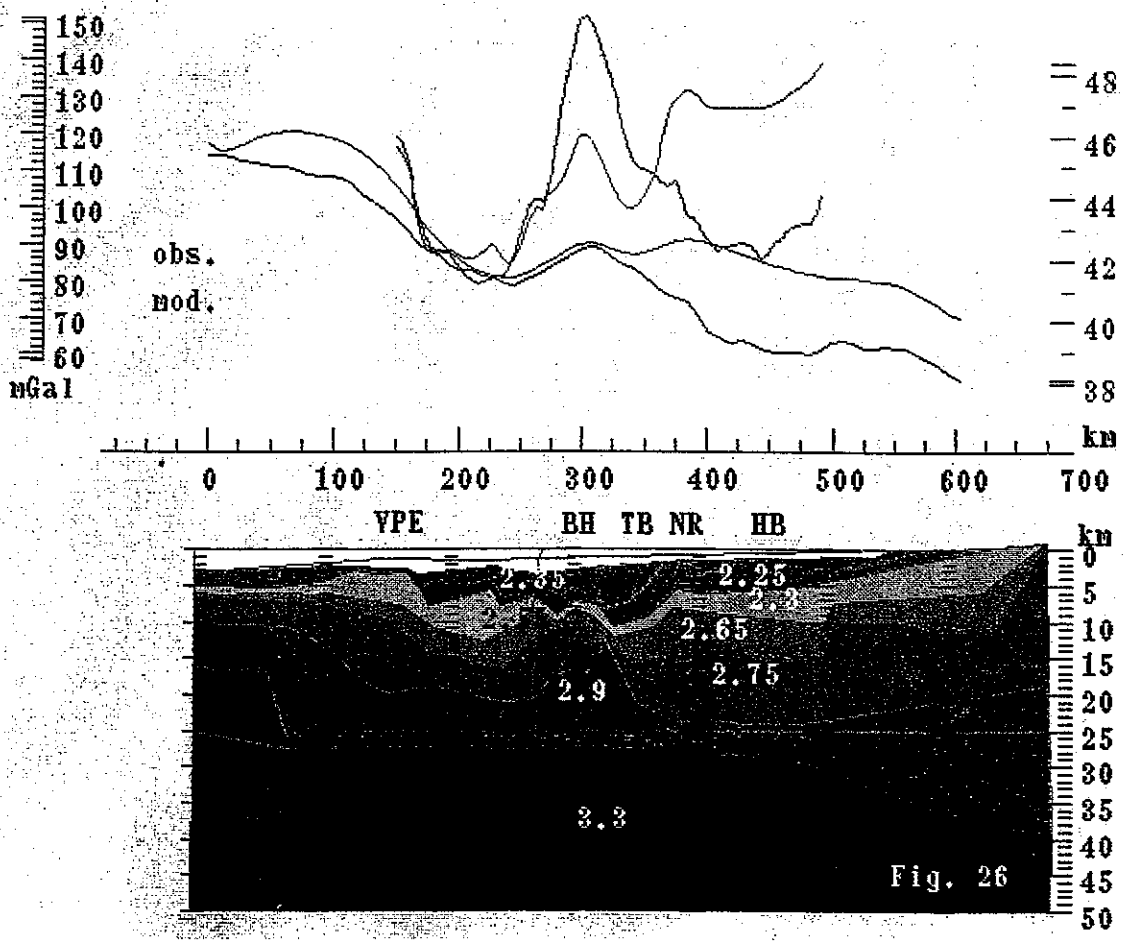
150
140
130
120
110
100
90
80
70
60
mGal
obs.
mod.
48
46
44
42
40
38
km
0
100
200
300
400
500
600
700
VPE
BH TB NR HB
km
2.35
2.25
2.3
2.65
2.75
2.9
3.3
0
5
10
15
20
25
30
35
40
45
50

Fig. 26

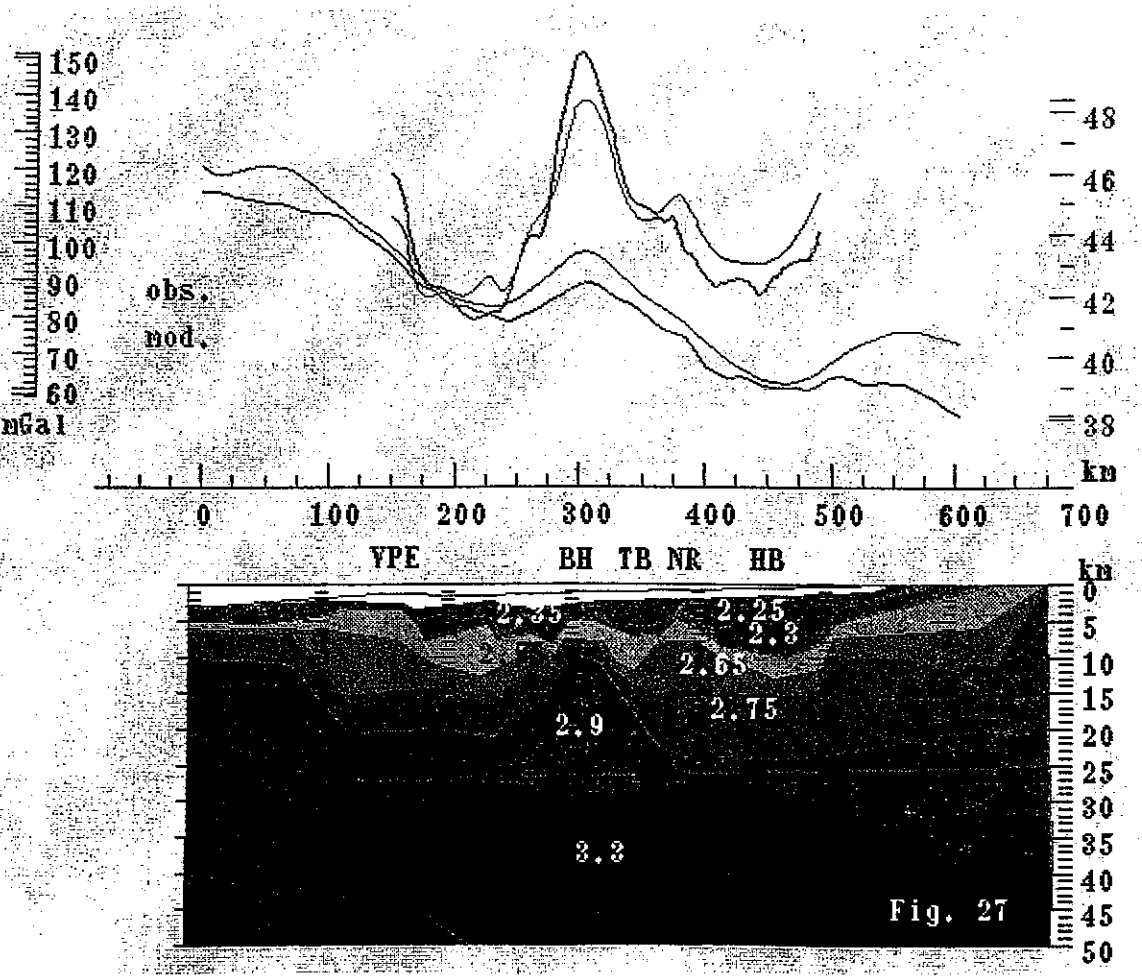
150
140
130
120
110
100
90
80
70
60
mGal
obs.
mod.
48
46
44
42
40
38
km
0
100
200
300
400
500
600
700
VPE
BH TB NR HB
km
2.35
2.25
2.3
2.65
2.75
2.9
3.3
0
5
10
15
20
25
30
35
40
45
50

Fig. 27

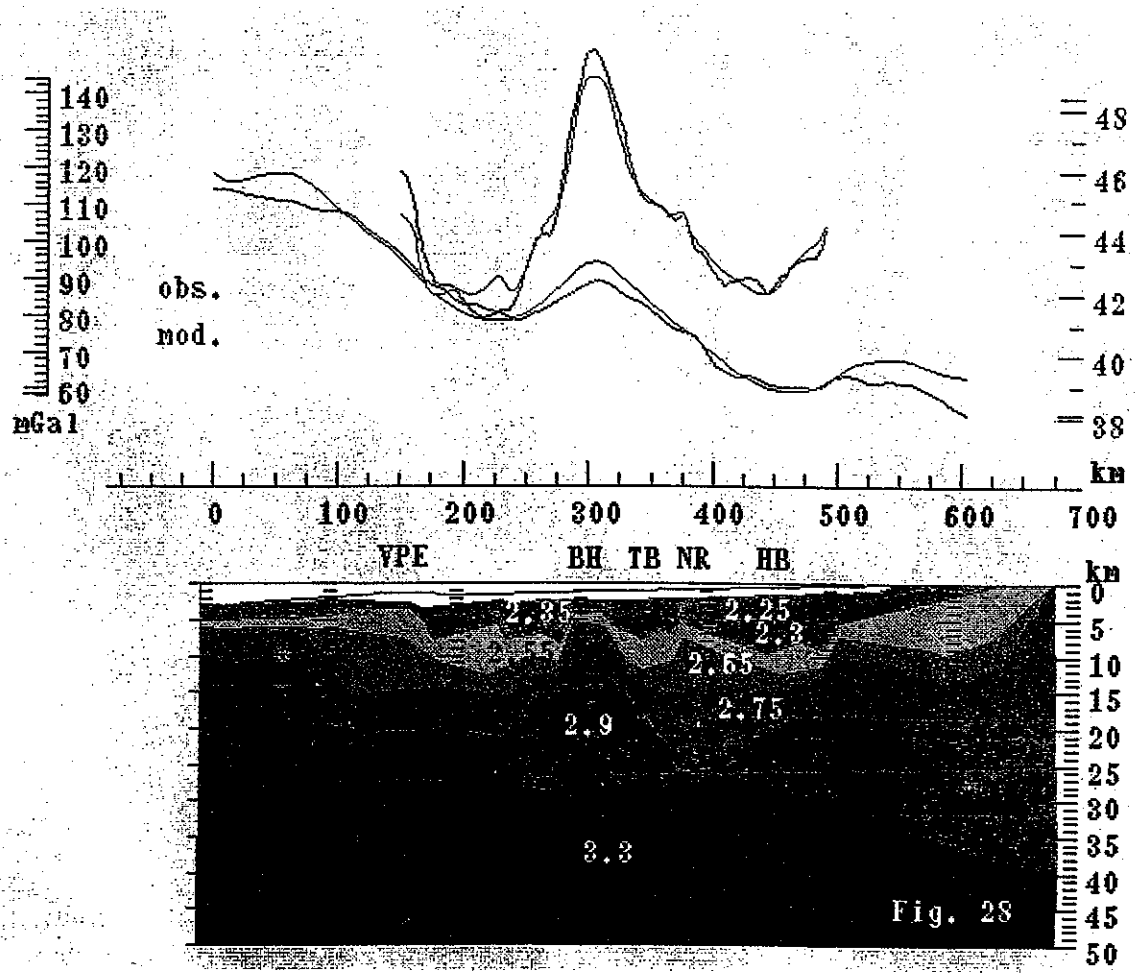
140
130
120
110
100
90
80
70
60
mGal
obs.
mod.
48
46
44
42
40
38
km
0
100
200
300
400
500
600
700
VPE
BH TB NR HB
km
2.85
2.25
2.3
2.55
2.65
2.75
2.9
3.3
0
5
10
15
20
25
30
35
40
45
50

Fig. 28